

PT-Symmetric Plasmonic Metamaterials

Hadiseh Alaeian^{1,2} and Jennifer A. Dionne²

¹*Department of Electrical Engineering, Stanford University, Stanford, California 94305, USA*

²*Department of Materials Science and Engineering,
Stanford University, Stanford, California 94305, USA*

We theoretically investigate the optical properties of parity-time (*PT*) symmetric three-dimensional metamaterials composed of strongly-coupled planar plasmonic waveguides. By tuning the loss-gain balance, we show how the initially isotropic material becomes both asymmetric and unidirectional. Investigation of the band structure near the material's exceptional point reveals several intriguing optical properties, including double negative refraction, Bloch power oscillations, unidirectional invisibility, and reflection and transmission coefficients that are simultaneously equal to or greater than unity. The highly tunable optical dispersion of *PT*-symmetric metamaterials provides a foundation for designing an entirely new class of three-dimensional bulk synthetic media, with applications ranging from lossless sub-diffraction-limited optical lenses to non-reciprocal nanophotonic devices.

Textbook conceptions of light-matter interactions have been challenged by two recent material advances — the development of metamaterials and the discovery of parity-time *PT*-symmetric media. Metamaterials allow considerable control over the electric and magnetic fields of light, so that permittivities, permeabilities, and refractive indices can be tuned throughout positive, negative, and near-zero values. Metamaterials have enabled negative refraction, optical lensing below the diffraction limit of light and invisibility cloaking [1–9]. Complementarily, *PT*-symmetric media allow control over electromagnetic field distributions in loss and gain media, so that light propagation can be asymmetric and even unidirectional. *PT*-symmetric media have enabled loss-induced optical transparency, lossless Talbot revivals and unidirectional invisibility [10–21]. Combined with non-linear media, they have also been suggested as optical diodes, insulators, circulators, and perfect cavity absorber-lasers [22–28].

While metamaterials rely on subwavelength engineered ‘building blocks’ to control electric and magnetic light-matter interactions, *PT*-symmetric media rely on judicious spatial arrangement of loss and gain media. Their unique asymmetric properties are based on a fundamental insight from quantum mechanics indicating that Hamiltonians need not be Hermitian to yield real eigenvalues and hence physical observables. Instead, the weaker condition of parity and time symmetry is sufficient to yield real eigenvalues below a certain threshold. Above this threshold, eigenvalues move into the complex plane and become complex conjugates of each other [29–33].

In the context of optics, *PT*-symmetric Hamiltonians arise from the duality between the quantum mechanical Schrodinger equation and the wave equation. Provided the refractive index profile satisfies $n(x) = n^*(-x)$, light will propagate as if it experiences a *PT*-symmetric potential. Below the *PT*-symmetric exceptional point, the optical eigenvalues will be purely real; however, as the

loss and gain of the material are increased beyond the exceptional point, the eigenvalues will become complex. In particular, certain eigenmodes will experience increased loss while other eigenmodes will exhibit strong optical gain. This behavior is at the core of the asymmetric and unidirectional optical properties observed in *PT* media to date.

While nearly all *PT*-symmetric media have been constructed from macroscopic (i.e., greater than wavelength-scale) elements, the optical Hamiltonian places no restrictions on the length scales over which the index profile can vary. This insight drives the question: can we create *PT*-symmetric metamaterials — i.e., bulk photonic media whose optical properties are determined both by their subwavelength building blocks and a judicious choice of their loss/gain profile? Such metamaterials would enable unprecedented control over electric and magnetic optical fields across wavelength and subwavelength scales, and may enable an entirely new class of bulk synthetic photonic media.

In this Letter, we investigate the emergent optical properties of bulk, three-dimensional *PT*-symmetric metamaterials. As a prototype metamaterial, we consider a multilayer stack of alternating layers of metal and dielectric. Both theoretical [34] and experimental [6] work has demonstrated the isotropic negative index response of this metamaterial, resulting in all-angle negative refraction and Veselago ‘perfect optical lensing.’ Its operation is based on the negative index plasmonic modes of its unit cell — a five-layer ‘metal-insulator-metal’ waveguide. By varying the thickness of the layers as well as the materials, the frequency of operation and the emergent bulk index of refraction can be precisely controlled throughout optical frequencies. While practical utilization of this negative index metamaterial has been limited by propagation and coupling losses, we will show that these losses could be overcome by subjecting the plasmonic modes to *PT*-symmetric potentials. Moreover, *PT*-symmetric potentials in this metamate-

rial can enable above-unity transmission and reflection, Bloch power oscillations, hyperbolic to elliptic dispersion transitions, and unidirectional invisibility.

Figure 1a illustrates the specific plasmonic metamaterial investigated in this paper, with the unit cell period indicated by Λ . Within each unit cell, the thicknesses of the metal t_m and dielectric t_d are deeply subwavelength, with $t_m = t_d = 30$ nm. We consider Ag as the metal, described by a lossless Drude model with dielectric constant $\epsilon_{Ag} = 1 - (\frac{\omega_p}{\omega})^2$ [35]. The bulk plasma frequency of Ag, ω_p , is assumed to be $8.85 \times 10^{15} \text{s}^{-1}$. We consider the dielectric layers to be TiO_2 with $n = 3.2$. With these materials, the surface plasmon resonance, ω_{sp} , occurs at 1.73 eV ($\omega_{sp}/\omega_p = 0.29$), and negative index modes are observed between this frequency and ω_p . This particular materials combination was recently experimentally shown to exhibit all-angle negative refraction and Veselago lensing [6]. Here, we theoretically investigate the evolution of the optical bands of this metamaterial upon varying the imaginary part of the refractive index of TiO_2 , denoted as k in Fig. 1. PT -symmetric potentials require balanced loss and gain, so the magnitude of this ‘non-Hermiticity parameter’, k , is identical for alternating dielectric layers.

Using the transfer matrix approach described in [36], we solve for the dispersion curves of the five-layer unit-cell plasmonic waveguide for transverse-magnetic (TM) polarized illumination. To determine the band diagrams of the periodic metamaterial, the wavevector along the z -direction is swept in the first Brillouin zone, $(0, \frac{\pi}{\Lambda})$, and the characteristic equation is minimized to find the propagation constant along the x -direction at each frequency. The results are shown in panels (b)-(e) of Fig. 1 for $k = 0, 0.2, 0.3$ and 0.5 , respectively. Note that the colormap indicates purely real values of k_x , corresponding to lossless propagation along the metamaterial. For a non-Hermiticity parameter $k = 0$, four different branches are observed: two below ω_{sp} (B_1 and B_2) and two above (B_3 and B_4). Because all constituents are lossless, the wavevectors diverge at ω_{sp} . B_1 and B_2 are characterized by positive slopes and hence positive refractive mode indices. In contrast, B_3 and B_4 are characterized by negative slopes and hence negative refractive mode indices.

When the non-Hermiticity parameter of the metamaterial is increased, the modes merge together at the exceptional points of the dispersion, denoted by black circles in panels (c)-(e). Beyond these exceptional points, the two distinguishable lossless modes below and above ω_{sp} (i.e., B_1 and B_2 or B_3 and B_4 , respectively) evolve to a gain mode and a loss mode with the same phase velocity. Due to their complex wavevectors, we denote these modes as black, dashed lines in Fig. 1(c)-(e). To understand these loss and gain modes, note that the transfer matrix of the PT -symmetric metamaterial possesses the following symmetry property:

$$T(\omega, k_z, k_x^*) T^*(\omega, k_z, k_x) = I \quad (1)$$

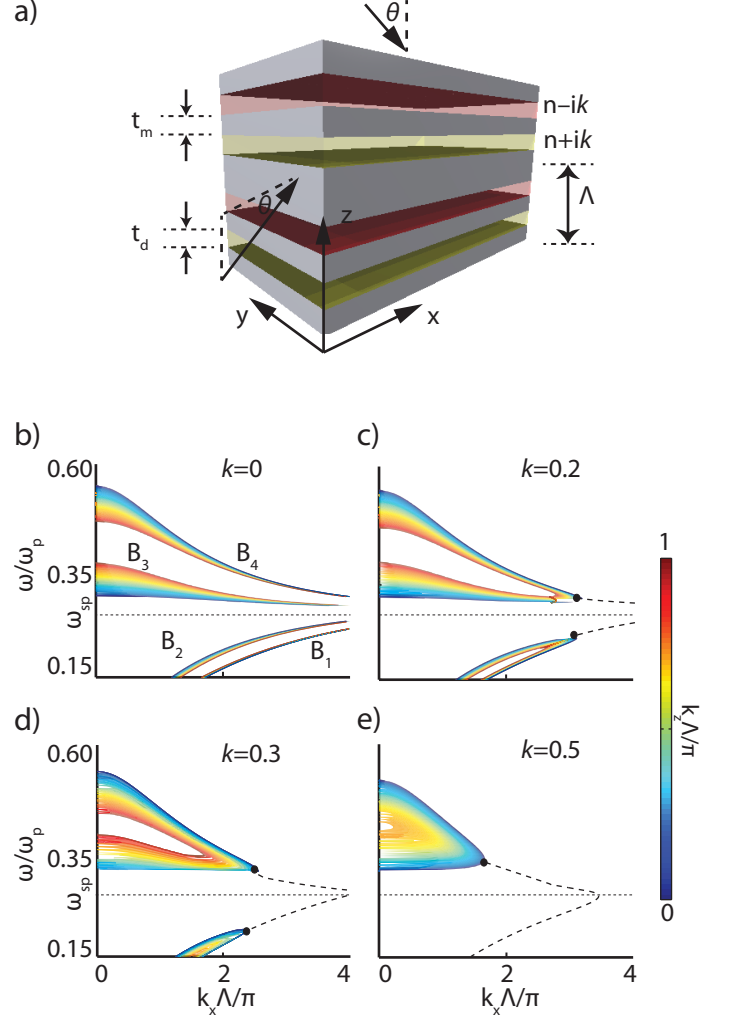


FIG. 1. Schematic of the plasmonic metamaterial (a), and the associated band diagrams for transverse magnetic modes (TM). The metamaterial is composed of coupled plasmonic waveguides, with deeply subwavelength metal and dielectric thicknesses of $t_m = t_d = 30$ nm. The unit-cell period is $\Lambda = 150$ nm. The refractive index of the dielectric is $n \pm ik$, with $n = 3.2$ and k corresponding to the non-Hermiticity parameter. Band diagrams are included for $k = 0$ (b), 0.2 (c), 0.3 (d) and 0.5 (e). Bands B_1 and B_2 are positive refractive index bands, while bands B_3 and B_4 correspond to negative refractive index bands. The horizontal dotted black lines in panels (b)-(e) indicate the surface plasmon resonance frequency, ω_{sp} . The black circles in panels in the same panels indicate the exceptional points of the dispersion, beyond which the purely real modes evolve to the complex modes characterized by either loss or gain (dashed black lines).

where I is the identity matrix. The Bloch modes of the metamaterial are eigenvalues of T and satisfy:

$$|T(k_x) - e^{i\Lambda k_z} I| = 0 \quad (2)$$

Taking the complex conjugate of Eq. 2 and using the symmetry property of Eq. 1, the following relation is ob-

tained:

$$|T(k_x^*) - e^{i\Lambda k_z} I| = 0 \quad (3)$$

Equation 3 means that if k_x (a complex number in general) admits a real solution for the Bloch wavevector, k_x^* is a solution for that Bloch mode as well. Accordingly, the bands have centro-symmetry in the complex (k_x, k_z) plane. Also note that the loss and gain modes of Fig. 1 (c)-(e) conjoin at ω_{sp} ; further, unlike the modes for a zero non-Hermiticity parameter, their wavevectors at ω_{sp} remain finite.

While *real* periodic spatial refractive index profiles lead to the appearance of an infinite number of band gaps, *complex* periodic index profiles generally result in complex dispersion curves across the entire frequency range. Interestingly, if the refractive index profile satisfies the condition for *PT* symmetry ($n(z) = n^*(-z)$) real propagation constants and complete band gaps can exist provided $k \leq k_{th}$. Here, k_{th} is the threshold value at which the Hamiltonian and the *PT* operator no longer commute, and consequently, real-valued solutions cease to be supported by the complex potential. Fig. 1 (c)-(e) illustrate this feature for increasing non-Hermiticity parameter. For example, for $k = 0.2$ and $k = 0.3$ purely real wavevectors and bandgaps are observed for all bands both above and below ω_{sp} . However, for $k = 0.5$, purely real eigenmodes below ω_{sp} do not exist across visible and near-infrared frequencies. Further, the bandgap between B_3 and B_4 merges for large k_z , and these bands only exist over a very limited wavevector and wavelength range.

The non-Hermiticity parameter not only changes the propagation constant and bandgap of the metamaterial, but also the band curvature. Fig. 2 plots the equi-frequency contours of bands B_1 - B_4 at wavelengths of $\lambda = 954$ nm ($\omega/\omega_p = 0.22$) for B_1 and B_2 , $\lambda = 604$ nm ($\omega/\omega_p = 0.35$) for B_3 , and $\lambda = 445$ nm ($\omega/\omega_p = 0.48$) for B_4 . Since the metamaterial is isotropic in the xy -plane and the contours are centro-symmetric in the (k_z, k_x) plane, a quadratic dispersion relation $(\frac{k_x}{n_x})^2 + (\frac{k_z}{n_z})^2 = k_0^2$ can be used to model the bands. Here k_0 indicates the free-space wavevector. The fitted refractive mode indices are listed in Table I.

	$k = 0$	$k = 0.2$	$k = 0.5$
	(n_x^2, n_z^2)	(n_x^2, n_z^2)	(n_x^2, n_z^2)
B_1	(95.86, 289.89)	(85.5, 53.56)	NA
B_2	(54.14, -58.86)	(59.32, -24.83)	NA
B_3	(-4.11, 1.27)	(-4.88, 1.21)	(11.55, 1.16)
B_4	(1.9, 1.85)	(1.85, 1.45)	(1.02, 0.66)

TABLE I. Effective refractive indices of the four bands based on a quadratic fit. The parameters are calculated for wavelengths of $\lambda = 954$ nm (B_1, B_2), 604 nm (B_3) and 445 nm (B_4).

As seen both in Fig. 2 and Table I, for a non-

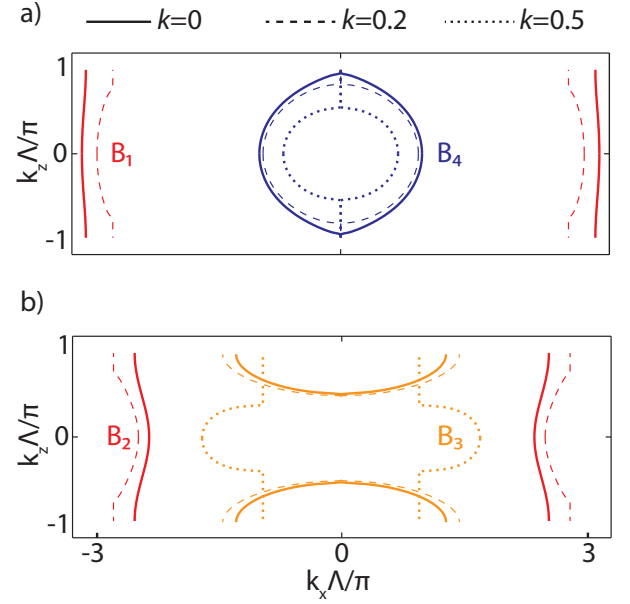


FIG. 2. Equi-frequency contours of the metamaterial, plotted for both positive and negative index bands at wavelengths of $\lambda = 954$ nm (B_1, B_2), 604 nm (B_3) and 445 nm (B_4). Band B_4 is circular for zero and small k , corresponding to an isotropic metamaterial. For all k , bands B_1 and B_4 remain elliptical while band B_2 is hyperbolic. However, band B_3 undergoes a hyperbolic to elliptical transition with increasing k .

Hermiticity parameter $k = 0$, bands B_1 and B_4 are elliptical (i.e., $n_x^2 n_z^2 \geq 0$) while bands B_2 and B_3 are hyperbolic (i.e., $n_x^2 n_z^2 \leq 0$). Moreover, B_4 is characterized by a nearly-perfect circular equi-frequency contour and almost equal values of effective refractive indices in both the x and z -directions. Accordingly, this metal-insulator-metal metamaterial is isotropic at $\lambda = 445$ nm, consistent with prior work [6, 34].

For increasing non-Hermiticity parameter, B_1 and B_4 remain elliptical while B_2 remains hyperbolic. Interestingly, however, band B_3 undergoes a hyperbolic to elliptical transition for $k = 0.5$. Such hyperbolic-to-elliptic transitions could enable dynamic tuning of Purcell enhancements for emitters near the metamaterial. Further, they could modulate Talbot revivals or the formation and resolution of images generated by hyperbolic metamaterial super-lenses [37–41].

The results of Fig. 2 imply that with increasing non-Hermiticity parameter, the material can evolve from an isotropic metamaterial to an anisotropic one. Intriguingly, the structure can also become highly directional. This property cannot be derived from the band diagrams, but can be understood by considering the transfer matrix:

$$T = \begin{bmatrix} a & b \\ c & a^* \end{bmatrix} \quad (4)$$

Here, the parameters a , b and c are related to the reflec-

tion and transmission coefficients r and t as $r_L = -\frac{c}{a^*}$, $r_R = \frac{b}{a^*}$ and $t_L = t_R = \frac{1}{a^*}$, where the subscripts L and R denote illumination from the left and right, respectively. As these equations indicate, an optical system composed of linear and reciprocal materials is non-directional provided the components are lossless. In other words, the transmitted and reflected powers $T = |t|^2$ and $R = |r|^2$ sum to unity and are independent of illumination direction, since $T_L = T_R = T$ and $T + R_R = 1 = T + R_L$, so $R_L = R_R$. When loss or gain is introduced into the system, the transmission coefficient remains the same for both directions of illumination. However the reflection coefficient need not be symmetric, as power can be attenuated or generated within the structure. The asymmetry is obtained at the price of losing propagating Bloch modes. However, as we will show, asymmetric responses can be obtained in a PT -symmetric potential where purely real bands exist as well.

To illustrate this directional behavior, Fig. 3 plots plane-wave refraction of light from vacuum ($n = 1$) through a metamaterial composed of 10 unit cells. We consider TM-polarized illumination of wavelength $\lambda = 445$ nm impinging on the metamaterial at an angle of $\theta = 45^\circ$ in the (x, z) plane. The colormap of Fig. 3 plots the H_y component of the fields. The arrows of Fig. 3 indicate the direction of illumination, refraction and transmission, each determined by spatially-averaging the Poynting vector in each region.

For $k = 0$ (Fig. 3a), the power is negatively refracted with an angle of $\sim -32^\circ$. This result is in excellent agreement with our band structure calculations, which yield a refracted angle from Snell's law of $\sim -31^\circ$. The refractive index, $n = -\sqrt{1.87} = -1.36$, at this non-Hermiticity value is independent of the illumination angle and direction. Indeed, for illumination in the (x, z) plane, or an 'endfire configuration', the same refraction angle is observed (see Fig. 4a). The same refraction angle is also observed for illumination from all sides of the metamaterial (i.e., illumination from $\pm x$, $\pm y$, and $\pm z$)

Upon increasing the non-Hermiticity parameter of the metamaterial, the material becomes highly directional. Panels (b) and (c) of Fig. 3 illustrate the field profiles in a 10-layer PT -symmetric metamaterial when illumination is from the loss and gain side (i.e., illumination in the $+z$ or $-z$ directions, respectively). As a particular example, we consider $k = 0.445$. As seen, field profiles and refraction angles are completely different for illumination from $+z$ (loss side) versus $-z$ (gain side). Illumination from $+z$ yields negative refraction at an angle of $\sim -81^\circ$ (see Fig. 3b). In contrast, illumination from $-z$ yields negative refraction at an angle of $\sim -43^\circ$ (Fig. 3c).

More intriguingly, this structure is characterized by tunable reflection and transmission coefficients that can range from zero to at or above unity. This characteristic is illustrated in the lower panels of Fig. 3, which plot the normalized-to-incidence power at each position along the

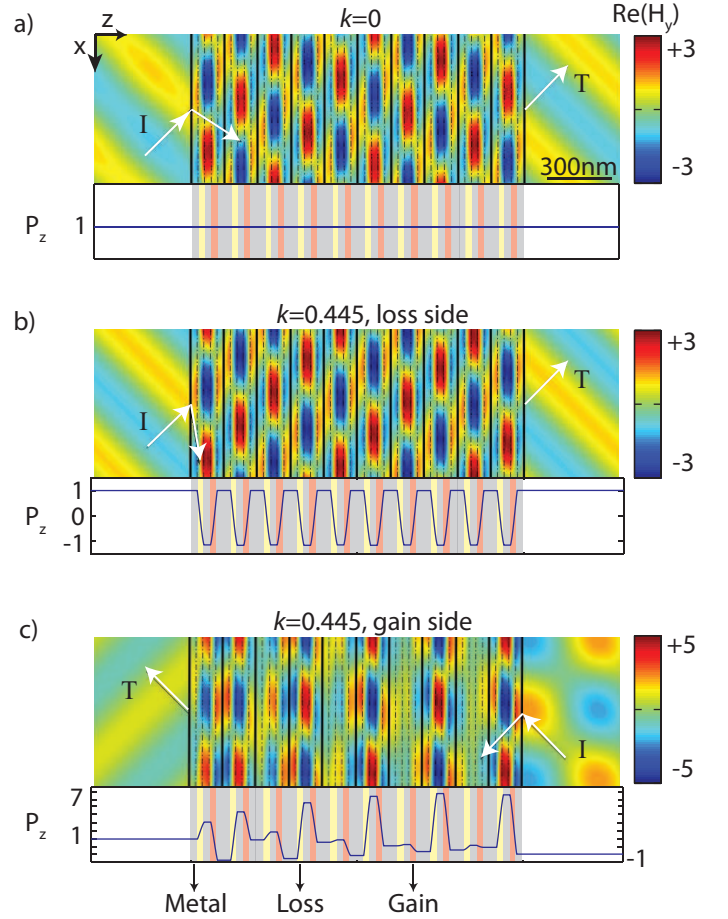


FIG. 3. $\text{Re}(H_y)$ for a 10-unit-cell metamaterial upon illumination by a planewave in air of wavelength $\lambda = 445$ nm and angle $\theta = 45^\circ$. Panel (a) shows the results for $k = 0$ while (b) and (c) show the results for $k = 0.445$ when illuminated from loss ($+z$) and gain ($-z$) side, respectively. The overlaid arrows indicate the direction of the averaged Poynting vectors in the corresponding regions. I in each panel indicates the incident wavevector while T shows the transmitted planewave. The lower graphs in each panel show the distribution of the power in each layer of the stack. The metallic layer is represented in gray, while the gain and loss regions are represented in red and yellow, respectively.

direction of propagation. For example, for illumination from the $-z$ direction (panel (c)) power flows backward toward the source in the illumination region ($P_z = -1$), and away from the metamaterial on the transmission side ($P_z = +1$). Therefore, the metamaterial is completely transparent, in that the metamaterial can transmit all of the incident power, even though light is emitted back towards the source.

Moreover, for illumination from the $+z$ direction (panel (b)) this metamaterial can achieve unidirectional invisibility. As seen, the power is unity on both sides of the metamaterial, indicating complete suppression of reflection on the illumination side and complete trans-

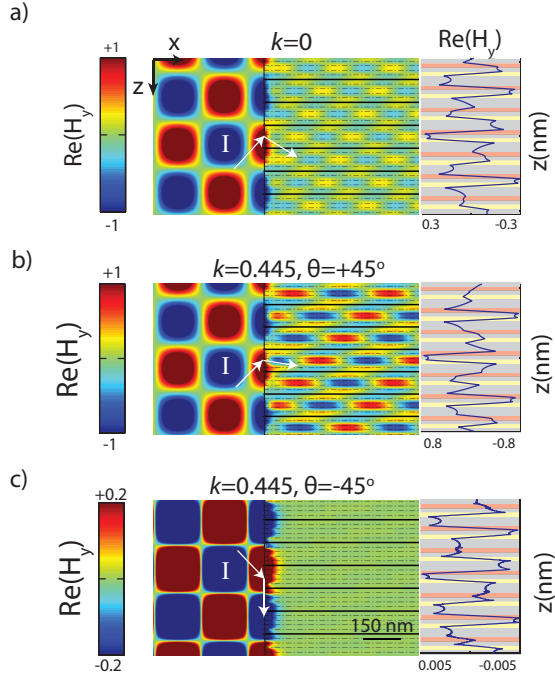


FIG. 4. $\text{Re}(H_y)$ when a semi-infinite metamaterial is illuminated with a planewave at $\lambda = 445$ nm along x -direction (endfire illumination). The illumination angle θ equals 45° in (a) and (b) and -45° in (c). The side graphs in each panel show the distribution of the magnetic field $1\mu\text{m}$ away from the interface.

mission on the other. Formally, perfect invisibility requires that the transmitted phase (ϕ_t) equal the phase of a planewave propagating in free-space (ϕ_{FS}). For the 10-layer metamaterial of Fig. 3b, $\frac{\phi_{FS}-\phi_t}{2\pi} = 2.75$, so the object could be identified through the interference with a reference planewave. However, perfect unidirectional invisibility, i.e. $\phi_{FS} - \phi_t = 2m\pi$ where m is an integer, can be achieved when the number of periods is increased to 55, 74 and 91.

The unusual directional scattering properties of the metamaterial can be rationalized by considering the power as light propagates through the array. For $k = 0$, power remains constant throughout the metamaterial (Fig. 3a). However, with increasing k , power begins to oscillate within the metamaterial, with power increasing in the gain regions and decreasing in the loss regions. These plasmonic power oscillations are analogous to Bloch oscillations observed in both electronic and photonic crystals [42] as well as PT-symmetric arrays [22].

As a final visual example of the unusual unidirectional properties of this metamaterial, Fig. 4 plots the fields and refracted angles for illumination along the $+x$ direction (endfire illumination). For a non-Hermiticity parameter $k = 0$, illumination at $\theta = \pm 45^\circ$ yields refraction at $\mp 30^\circ$, respectively, in good agreement with the previously determined value of $\mp 31^\circ$. With increasing non-Hermiticity

parameter, however, illumination at $+\theta$ yields markedly different results than illumination at $-\theta$. For example, for $k = 0.445$, illumination at $+45^\circ$ yields a refracted angle of -11° , while illumination at -45° yields refraction along the metamaterial interface at an angle of -90° . This double refraction does not just manifest itself in the intensity of the transmitted beam, but also in the profile of the fields, as seen in the right panels of Fig. 4.

We now consider the effect of varying the non-Hermiticity parameter on the scattering properties of the metamaterial. As before, we consider TM-polarized illumination with a 45° tilted planewave at $\lambda = 445$ nm. We limit our analysis to illumination along either $+z$ ('left-side illumination (L)') or $-z$ ('right-side illumination (R)') Based on Eq. 1, a generalized energy conservation formula can be derived as $|T - 1| = \sqrt{R_R R_L}$, where T is the transmitted power and R_R and R_L are the reflected powers from the right and left sides, respectively [43].

Figure 5 plots the reflection and transmission coefficients as a function of k . As seen in Fig. 5d, for $k = 0.035$, the transmitted power equals unity independent of the number of layers. Correspondingly at this point R_R , shown in panel (b), vanishes for any number of layers. This property manifests itself as a peak in Fig. 4c, where the quotient of relative reflection coefficients is plotted. Importantly, for $k = 0.035$, this PT-symmetric metamaterial is still isotropic, characterized by circular equifrequency contours. Therefore, this PT-symmetric optical potential could enable lossless and far-field Vesalago lensing.

For larger non-Hermiticity parameters ($k > 0.035$), T exceeds unity. Interestingly, while the transmitted power varies with k and the number of unit cells, it never drops below 1 up through $k = 0.445$. At this non-Hermiticity value, the reflected power from the left/loss side (R_L) vanishes, as shown in Fig. 5a. For larger k , T remains at or below unity. Non-Hermiticity parameters k above 0.63 yield purely imaginary k_z , so no propagation is allowed through the metamaterial. This property is accompanied by a rapid drop in T and strong increase in the reflectance for any number of layer.

While for left- (or loss)-side illumination the reflection coefficient is always less than unity, for right- (or gain)-side illumination the reflected power can exceed 1. This behavior is not monotonic however, depending strongly on the number of unit-cell layers and k . Indeed, only at $k = 0$ and $k = 0.12$ are the reflected powers from the left and right identical and equal to unity. For $k > 0.12$, the ratio r_L/r_R remains below unity (Fig. 5c).

Table II summarizes some of the interesting scattering properties of the 10-unit-cell metamaterial extracted from Fig. 5. For $k = 0$, the metamaterial is Hermitian and lossless. With increasing PT-symmetric potentials, unusual features such as above unity transmission ($k = 0.26$), above unity reflection ($k = 0.445$) and uni-

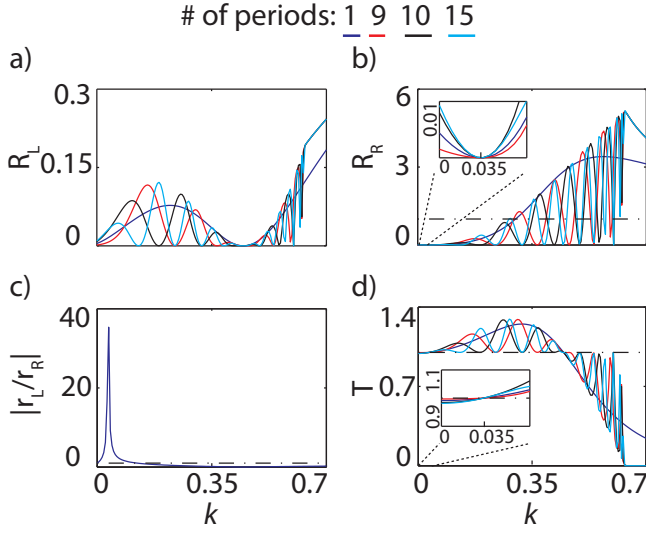


FIG. 5. Reflected and transmitted powers of the metamaterial with increasing k and varying numbers of periods. (a) Reflected power upon illumination from the left (loss) side of the metamaterial; (b) reflected power upon illumination from the gain (right) right side; (c) Quotient of reflected powers; (d) Transmitted power. In all panels, the incident angle is $\theta = 45^\circ$ and the illumination wavelength is $\lambda = 445$ nm. The inset in panel (b) and (d) show the behavior of the reflected and transmitted powers around $k = 0.035$ where R_R vanished and $T = 1$ independent of the number of periods.

directional reflection suppression ($k = 0.445$ and $k = 0.5$) are observed. The normalized Bloch wavevector for each k is included in the last row of the table. Since k_z is purely real, light propagates in a pass band of the metamaterial for all of these non-Hermiticity parameters.

	$k = 0$	$k = 0.035$	$k = 0.26$	$k = 0.445$	$k = 0.5$
R_L	0.0080	0.03	0.0982	0	5×10^{-4}
R_R	0.0080	0	0.8397	2	0.1219
T	0.9920	1	1.2872	1	0.9922
$\frac{\Delta k_z}{\pi}$	0.7633	0.7609	0.6502	0.4683	0.3948

TABLE II. Transmitted and reflected powers from left and right and the normalized Bloch wavevector for 10-unit-cell metamaterial at $\lambda = 445$ nm and $\theta = 45^\circ$.

In conclusion, we have introduced the concept of a PT -symmetric metamaterial. The original lossless metamaterial, composed of a periodically-stacked 5-layer plasmonic waveguide, was designed to behave as an isotropic, three-dimensional negative refractive index material. By subjecting the plasmonic modes to PT -symmetric optical potentials, we demonstrated the broad tunability of the band curvatures, band gaps and effective refractive indices of the material. Small but non-zero non-Hermiticity parameters increased the transmission of the isotropic negative index metamaterial to unity. Larger non-Hermiticity parameters morphed the material from

isotropic to anisotropic and directional. The highly unusual optical properties of PT -symmetric metamaterials could be used to devise an entirely new class of bulk synthetic media, ranging from lossless Veselago lenses to unidirectional metamaterial-based invisibility cloaks and new non-reciprocal nanophotonic devices.

Useful discussions and feedback from Dionne Group members are highly appreciated. This work is supported in part by a SLAC National Accelerator Laboratory LDRD award in concert with the Department of Energy, Office of Basic Energy Sciences, Division of Materials Sciences and Engineering, under contract DE-AC02-76SF00515. Funding from the Hellman Faculty Scholars program and a National Science Foundation CAREER Award (DMR-1151231) are also gratefully acknowledged.

- [1] J. Valentine, S. Zhang, T. Zentgraf, E. U. Avila, D. A. Genov, G. Bartal, and X. Zhang, *Nature* **455**, 376 (2008).
- [2] J. Yao, Z. Liu, Y. Liu, Y. Wang, C. Sun, G. Bartal, A. M. Stacy, and X. Zhang, *Science* **321**, 930 (2008).
- [3] S. Zhang, D. A. Genov, Y. Wang, M. Liu, and X. Zhang, *Phys. Rev. Lett.* **101**, 047401 (2008).
- [4] S. Zhang, Y. S. Park, J. Li, X. Lu, W. Zhang, , and X. Zhang, *Phys. Rev. Lett.* **102**, 023901 (2009).
- [5] A. C. Atre, A. G.-Etxarri, H. Alaeian, and J. A. Dionne, *Adv. Optical Mater* **1**, 327 (2013).
- [6] T. Xu, A. Agrawal, M. Abashin, K. J. Chau, and H. J. Lezec, *Nature* **497**, 470 (2013).
- [7] V. M. Shalaev, *Nat. Photonics* **1**, 41 (2007).
- [8] C. M. Soukoulis and M. Wegener, *Nat. Photonics* **5**, 523 (2011).
- [9] H. J. Lezec, J. A. Dionne, and H. A. Atwater, *Science* **316**, 430 (2007).
- [10] H. Benisty, A. Degiron, A. Lupu, A. D. Lustrac, S. Chnais, S. Forget, M. Besbes, G. Barbillon, A. Bruyant, S. Blaize, and G. Lrondel, *Opt. Express* **19**, 18004 (2011).
- [11] A. Guo, G. Salamo, D. Duchesne, R. Morandotti, M. Volatier-Ravat, V. Aimez, G. Siviloglou, and D. Christodoulides, *Phys. Rev. Lett.* **103**, 093902 (2009).
- [12] H. Ramezani, D. N. Christodoulides, V. Kovanis, I. Vitebskiy, and T. Kottos, *Phys. Rev. Lett.* **109**, 033902 (2012).
- [13] K. Makris, R. El-Ganainy, and D. Christodoulis, *Phys. Rev. A* **81**, 063807 (2010).
- [14] M. C. Zheng, D. N. Christodoulides, R. Fleischmann, and T. Kottos, *Phys. Rev. A* **82**, 010103 (2010).
- [15] S. Longhi, *J. Phys. A: Math Theor* **44**, 485302 (2011).
- [16] C. E. Rter, K. G. Makris, R. El-Ganainy, D. N. Christodoulides, M. Segev, and D. Kip, *Nat. Phys.* **6**, 192 (2010).
- [17] Z. Lin, H. Ramezani, T. Eichelkraut, T. Kottos, H. Cao, and D. N. Christodoulides, *Phys. Rev. Lett.* **106**, 213901 (2011).
- [18] A. Mostafazadeh, *Phys. Rev. A* **87**, 012103 (2013).
- [19] L. Feng, Y. L. Xu, W. S. Fegadolli, M. H. Lu, J. E. Oliveira, V. R. Almeida, Y. F. Chen, and A. Scherer,

- Nat. Mater **12**, 108 (2013).
- [20] K. G. Makris, R. El-Ganainy, D. N. Christodoulides, and Z. H. Musslimani, Phys. Rev. Lett. **100**, 103904 (2008).
 - [21] G. Castaldi, S. Savoia, V. Galdi, A. Alu, and N. Engheta, Phys. Rev. Lett. **110**, 173901 (2013).
 - [22] Z. H. Musslimani, K. G. Makris, R. El-Ganainy, and D. N. Christodoulides, Phys. Rev. Lett. **100**, 030402 (2008).
 - [23] N. Lazarides and G. Tsironis, Phys. Rev. Lett. **110**, 053901 (2013).
 - [24] C. Li, C. Huang, H. Liu, and L. Dong, Opt. Lett. **37**, 4543 (2012).
 - [25] Y. He, X. Zhu, D. Mihalache, J. Liu, and Z. Chen, Phys. Rev. A **85**, 013831 (2011).
 - [26] S. V. Dmitriev, A. A. Sukhorukov, and Y. S. Kivshar, Opt. Lett. **35**, 2976 (2010).
 - [27] Y. D. Chong, L. Ge, and A. D. Stone, Phys. Rev. Lett. **106**, 093902 (2011).
 - [28] S. Longhi, Phys. Rev. A **82**, 031801 (2010).
 - [29] C. M. Bender, G. V. Dune, and P. N. Meisinger, Phys. Lett. A **252**, 272 (1999).
 - [30] C. M. Bender, Rep. Prog. Phys. **70**, 947 (2007).
 - [31] Z. Ahmed, Phys. Lett. A **282**, 343 (2001).
 - [32] C. M. Bender and S. Boettcher, Phys. Rev. Lett. **80**, 5243 (1998).
 - [33] A. Mostafazadeh, J. Math. Phys. **43**, 2814 (2002).
 - [34] E. Verhagen, R. de Waele, L. Kuipers, and A. Polman, Phys. Rev. Lett. **105**, 223901 (2010).
 - [35] Here we assume a lossless Drude model, but the results are generalizable to a realistic case including loss. See for example reference [10].
 - [36] P. S. J. Russell, T. A. Birks, and F. D. Lloyd-Lucas, Confined Electrons and Photons (1995).
 - [37] X. Ni, G. Naik, A. Kildishev, Y. Barnakov, A. Boltasseva, and V. Shalaev, Appl. Phys. B **103**, 553 (2011).
 - [38] Z. Jacob, I. I. Smolyaninov, and E. E. Narimanov, App. Phys. Lett. **100**, 181105 (2012).
 - [39] K. J. Webb and M. Yang, Opt. Lett. **31**, 2130 (2006).
 - [40] J. Kim, V. Drachev, Z. Jacob, G. Naik, A. Boltasseva, E. Narimanov, and V. Shalaev, Opt. Express **20**, 81008116 (2012).
 - [41] W. Zhao, X. Huang, and Z. Lu, Opt. Express **19**, 15297 (2011).
 - [42] R. Sapienza, P. Costantino, and D. Wiersma, Phys. Rev. Lett. **91**, 263902 (2003).
 - [43] L. Ge, Y. Chong, and A. Stone, Phys. Rev. A **85**, 023802 (2012).